Vol. 30, No. 6, November–December 1993

Aerobrake Design Studies for Manned Mars Missions

M. Tauber,* M. Chargin,† and W. Henline‡
NASA Ames Research Center, Moffett Field, California 94035
A. Chiu† and L. Yang§
Sterling Software, Palo Alto, California 94303
and
K. R. Hamm Jr.¶ and H. Miura**
NASA Ames Research Center, Moffett Field, California 94035

The vehicle's mass fractions that must be devoted to the aerobrakes, including the heatshields, have been computed for a high-speed manned Mars entry of 8.6 km/s and with a 5 Earth *g* deceleration limit. Blunt, low lift-to-drag (*L/D*) ratio configurations with ballistic coefficients (m/C_DA) of 100 and 200 kg/m^2 have been studied. In addition, a delta-winged vehicle, with a medium *L/D* and a ballistic coefficient of 375 kg/m^2, has been studied. Both insulative, radiatively cooled heatshields and ablators have been considered. After adding heatshielding and optimizing the structure, the aerobrakes' total mass fractions (heatshield plus aerobrake mass divided by the vehicle's total mass) varied from about 15 to 13% for ballistic coefficients of 100 and 200 kg/m^2, respectively, for the blunt shapes and was slightly under 17% for the winged vehicle. The winged vehicle's aerobrake mass fraction was somewhat greater because the former's much higher ballistic coefficient resulted in more intense heating, thus requiring more thermal protection. The aerobrakes' mass fractions range from less than to slightly over the 15% value that is considered to make aerobraking indisputably superior to propulsive braking.

Nomenclature

A	= vehicle reference area for aerodynamic coefficients, m^2
C_D	= drag coefficient
C_L	= lift coefficient
D	= drag
g	= acceleration due to gravity at Earth
L	= lift
m	= vehicle mass, kg
Q	= total heat load, kJ/cm^2
r_n	= vehicle nose radius, m
V_E	= entry velocity
X	= distance along body surface, m
α	= angle of attack, deg
$\Delta\gamma_E$	= entry flight-path angle corridor width at 90-km altitude, deg

Introduction

MANY studies have shown that large weight and cost savings can be achieved by using atmospheric braking at Mars instead of decelerating propulsively.[1–5] The objective of the present study is to determine the vehicle's mass fraction (fraction of total vehicle mass at entry) that must be devoted to the aerobrake's structure and thermal protection system. Both low and medium lift-to-drag ratio (*L/D*) shapes are considered. An inertial reference entry speed of 8.6 km/s (8.4 km/s with respect to the rotating atmosphere) is considered. The entry velocity is representative of fast missions (14–16 months long) and is near the upper limit usually considered for manned Mars entries. Therefore, the aerobrakes' thermal protection and structural requirements are stringent.

The configuration of the aerobrake depends primarily on the *L/D* that is required to achieve an adequately large entry corridor and to observe physiologically realistic deceleration limits. Present guidance and control capabilities require an entry angle corridor width at Mars of at least 1 deg. A deceleration limit of 5 (Earth) *g* is used; this value was proposed by scientists at NASA Ames Research Center and has been substantiated subsequently.[6] Its use facilitates comparison with other studies of this mission. Furthermore, a peak deceleration of somewhat over 5 *g* was experienced by three Soviet cosmonauts during entry following an 8-month-long orbital mission in 1984. The cosmonauts suffered no ill effects and, supposedly, played tennis two days after landing. However, the cosmonauts were subjected daily to several hours of strenuous exercise while in orbit.[6]

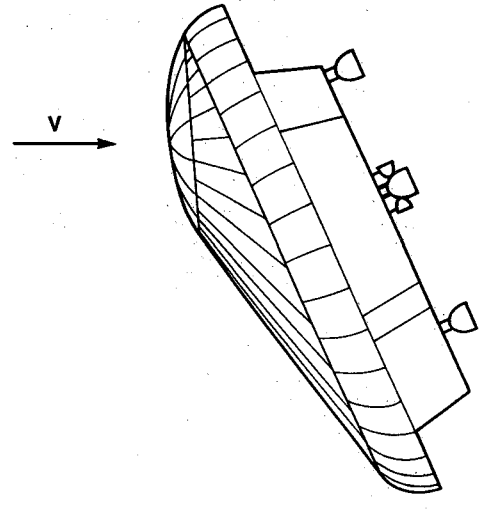

Fig. 1 AFE configuration showing aerobrake and payload.

Presented as Paper 91-1344 at the AIAA 26th Thermophysics Conference, Honolulu, HI, June 24–26, 1991; received July 5, 1991; revision received Jan. 4, 1993; accepted for publication Jan. 4, 1993.

*Research Scientist. Associate Fellow AIAA.
†Research Engineer. Member AIAA.
‡Research Scientist. Senior Member AIAA.
§Research Specialist.
¶Research Engineer.
**Aerospace Engineer. Associate Fellow AIAA.

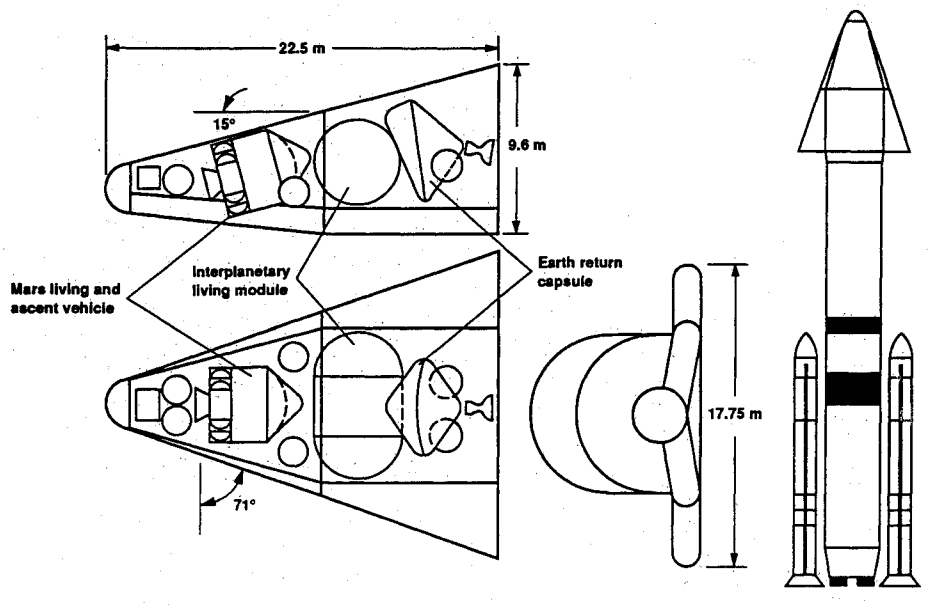

Fig. 2 Proposed Mars manned atmospheric braking vehicle.

First a blunted shape, based on the Aeroassist Flight Experiment (AFE) configuration (see Fig. 1), with a maximum L/D of 0.3 is considered. The aerobrake has a 26.7-m diameter. Two different ballistic coefficients (m/C_DA) have been chosen. The lower value of 100 kg/m^2 (about the same as the AFE) results in heating rates that are low enough to potentially use a radiatively cooled heatshield material such as advanced Shuttle tiles. For the second value of 200 kg/s^2, the heating rates are significantly higher and ablative heatshielding is needed.

In addition to the AFE configuration, a highly swept, delta-winged shape with a large-volume body is considered (see Fig. 2). Although the proposed Mars vehicle is an order of magnitude larger (22.5 m long), its configuration is based on and very similar to the shape tested under the Aerothermodynamic/Elastic Structural Systems Environmental Tests (ASSET) Program. (Six flight tests were made in air during the 1960s, at entry velocities of 4–6 km/s. Both aerodynamic and heat transfer data were measured and compared with ground-based facility tests and predictions. Therefore, an extensive data base exists.) This vehicle has an L/D of 0.85 at an angle of attack of 37 deg. The bottom windward surface experiences extensive turbulent boundary-layer flow and requires ablative heatshielding during Mars entry. Since winged vehicles have less drag than blunt shapes, their ballistic coefficients are larger, which results in a more intense and longer heating pulse, thus requiring more heatshielding. However, high L/D vehicles also have many advantages. For example, increasing the L/D from the AFE's value of 0.3 to 0.85 nearly doubles the entry flight-path angle corridor width and provides an order of magnitude increase in cross-range capability. The latter can be very important for descent from orbit. Finally, the winged vehicle has the potential of being launched into Earth orbit fully assembled. In contrast, the blunt shapes will probably have to be assembled in orbit, which may become a time-consuming, costly, and potentially hazardous procedure. It is envisioned that the primary crew compartment and the Earth entry capsule carried by the winged vehicle will be left in orbit for the return trip to Earth. The remainder of the winged vehicle will descend to the surface of Mars for the relatively brief stay of about 1 month, which is typical of fast missions. At the completion of the surface exploration period, a small ascent capsule will return the crew to orbit, and most of the winged vehicle will remain on the surface.

Analysis

The analysis consists of computing the entry trajectories and the heating and pressures at selected body locations. Next, the requirements of the thermal protection system (TPS) are found. The structural weight of the aerobrake shell is computed by optimizing the components consisting of beams and the honeycomb sandwich shell.

The atmospheric composition and structure that will be used is based on the Viking Mars lander measurements. The entry trajectories are computed at both the overshoot and undershoot boundaries using lift modulation. The lift is modulated by rolling the vehicle and thus rotating the lift vector while the angle of attack is held constant. It is necessary to find trajectories that assure high-speed atmospheric capture during a single pass since the vehicle enters at hyperbolic speed. Skip-out occurs at a speed of about 3.5 km/s to achieve an approximately circular orbit, which simplifies the descent to the planet's surface.

The heating of the vehicles is calculated at the stagnation point and other forebody locations. Laminar convective heating is computed assuming a pure CO_2 atmospheric composition for either a partially, or fully, catalytic surface using the methods described in Ref. 7. Since the vehicles are large, transitional and turbulent boundary-layer flow will occur. Boundary-layer transition correlations for air are used in the form presented in Ref. 8 but were modified to include transition information deduced from Shuttle flight measurements. The boundary-layer edge Mach number and Reynolds number are used in the correlations. (Studies of transition in fluids ranging from liquids to gases have shown the Reynolds number to be one of the primary parameters; this is the rationale for using air data in the absence of measurements in CO_2.) The length of the transitional flow region is taken to be the same as the preceding laminar flow. For turbulent boundary-layer heating, the expressions previously derived for air[9] (based on the reference enthalpy approximation) are used. In the heating relations described earlier, the boundary-layer edge conditions were correlated in terms of flight condition and body surface slopes to facilitate application of the method. The CO_2 transport properties of Ref. 10 are used in the computations.

Stagnation point equilibrium radiative heating is computed using an expression that is for a 97% CO_2 and 3% N_2 gas mixture.[11] The expressions[11] were derived from values computed using the code described in Ref. 12. The radiation off the stagnation point is calculated one dimensionally using the velocity component normal to the shock and the local shock-layer thickness. In general, only the blunt noses of the vehicles experience significant radiative heating. The radiative and convective heating are uncoupled in the computations. This assumption is valid if the radiative heating is much less than the total flow energy ($\frac{1}{2}\rho V^3$) and is

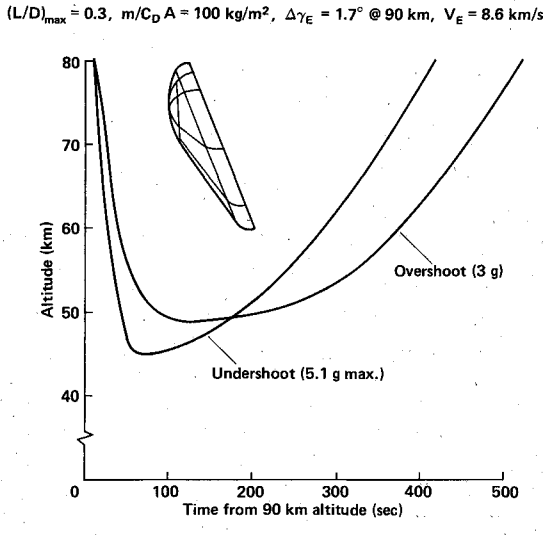

Fig. 3 Mars aerobraking trajectories for AFE-shaped vehicle.

applicable for the flight conditions considered here. Assuming that the radiation and convection are uncoupled implies that the boundary-layer edge temperature is only slightly reduced by radiative cooling; this assumption is plausible since the shock-layer radiative emission is a highly nonlinear function of temperature. All heating calculations are made assuming that the inviscid shock-layer flow is in thermochemical equilibrium.

The results of the previous heating calculations are used to find the thermal protection requirements. Time and manpower constraints prevented making extensive comparisions among different types of heatshield materials. For radiatively cooled, insulative types of materials such as reusable ceramic tiles, the surface insulation thickness is found[13] using the one-dimensional conduction model code SINDA, which stands for Systems Improved Numerical Differencing Analyzer.[14] A bond-line temperature of 533 K (500°F) is used and weight trades between tile and skin thickness are computed. Ablative heatshield materials are evaluated using the charring material ablation (CMA) code.[15] The CMA code couples the chemically reacting, laminar or turbulent boundary layer with a charring ablator. The computation is one dimensional but will provide both ablator and insulation thickness required to meet a specified backface temperature limit. Past studies of ablators suitable for manned vehicles[16] have led to the choice of relatively low density materials that also have low thermal conductivities since the heating pulses can last more than 5 min, as will be shown. Therefore, thermal protection materials having the aforementioned properties will be emphasized.

The structures of the aerobrakes are analyzed by using the peak values of the pressure over the windward portions of the bodies. Modified Newtonian theory is used to determine the pressure distribution. The maximum deceleration loads encountered during the aerobraking pass are also accounted for. The analysis was performed by using the MSC/NASTRAN code.[17] All primary structural members are assumed to be of polyimide/graphite (PI/Gr). However, the basic shell structure consists of an aluminum (2024) honeycomb sandwich core (having a specific gravity of 0.056) between PI/Gr face sheets; the shell is stiffened by I-beam frames. The material properties of PI/Gr are from Ref. 18. The payload is fastened to the blunt aerobrake shell at 12 connecting points that are assumed to be rigid supports. A maximum beam deflection limit of 20 cm (8 in.) is specified and honeycomb face sheet local buckling (wrinkling) limits are observed. On the winged vehicle, the center of mass of the payload is connected by a "wiffle-tree" arrangement to the front and aft (first and third) bulkheads, the location of which will be illustrated subsequently. The rigidity of the winged vehicle made it unnecessary to impose beam deflection limits. All allowable stresses and displacements are adjusted to provide a safety factor of 1.5 (which is standard for aircraft) giving a structural design load factor of 7.5 g for both vehicle configurations. A heatshield bond-line temperature limit of 533 K (500°F) is used. The structural components are optimized for minimum mass. Adding the heatshield mass and strain isolation pad (SIP) to the structural mass gives the net aerobrake mass. The total aerobrake mass is found by increasing the net value by 20–40% to account for fittings, hard-point fillings, joints, bolts, nuts, adhesives and coatings.

Results

Representative results will be shown that illustrate the trajectories, heating, heatshielding, and structural weight calculations. As previously outlined, the computations are for two different classes of configurations. The first shape to be considered is a scaled up version of the AFE; this configuration is representative of low L/D and low ballistic coefficient bodies. In contrast, the delta-winged vehicle has a medium L/D and a higher ballistic coefficient. Both AFE-shaped aerobrakes are assumed to be the same size. However, their payload is varied so that one has a total mass of 72.5 metric tons (mt) and the other 145 mt, giving ballistic coefficients of 100 and 200 kg/m^2, respectively. The value of 100 kg/m^2 results in heating rates that are potentially within the cooling capabilities of reusable surface insulation (i.e., ceramic tiles). The vehicle with the ballistic coefficient of 200 kg/m^2 experiences more severe heating and will require ablative heatshielding. (Another reason for considering ablative heatshields is that dust in the Martian atmosphere may severely damage the ceramic tiles' surfaces.[19] Therefore, the tiles may have to be coated with a heavy layer of protective material, or they may not be usable.)

It is assumed that the winged vehicle can, potentially, have a lower gross weight than a blunt shape. With a total mass that is estimated to be 57 mt, the winged configuration should have a mission capability similar to that of the 72 mt AFE shape. A primary reason for the lower weight is that the medium L/D, winged vehicle has adequate cross range and the potential capability to land on the planet. In contrast, a separate landing vehicle must be carried as part of the payload of a blunt aerobrake according to mission studies made by the Boeing Defense and Space Group,[20] partly because the blunt shapes have very limited cross range capability. (The cross range is proportional to L/D squared, to the first order, for L/D less than about 1.0.) Another reason for the smaller mass is the potentially greater structural efficiency of the fuselage of the winged vehicle that can be reinforced by the pressurized crew compartment(s); however, this benefit is neglected in the structural weight calculations to be conservative.

Trajectories

Both overshoot and undershoot aerobraking trajectories have been calculated for all three cases of interest here. Lift modulation is used throughout the entry. The overshoot trajectory is determined by the maximum lift of the vehicle and the undershoot flight

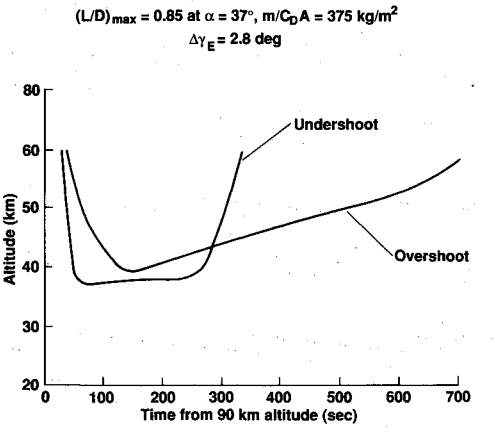

Fig. 4 Mars aerobraking trajectories for delta-winged vehicle.

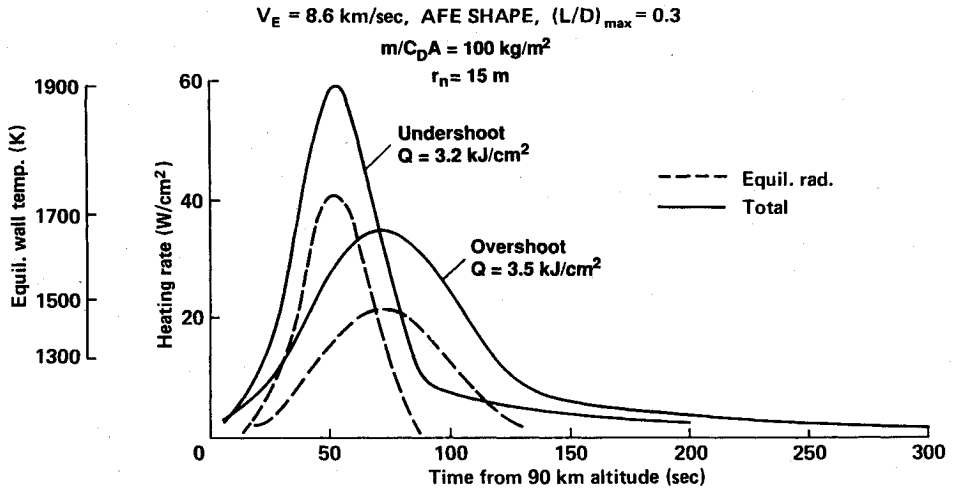

Fig. 5 Stagnation point heating pulses on AFE shape (m/C_DA = 100 kg/m²).

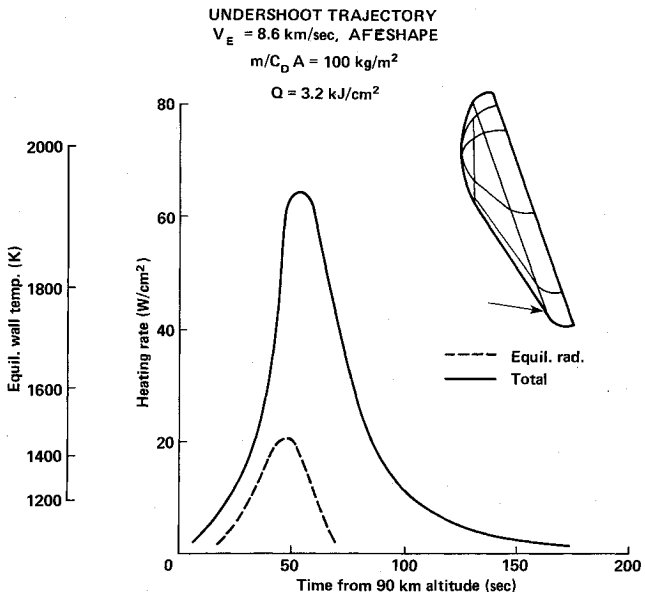

Fig. 6 Heating pulses on bottom of cone forebody centerline.

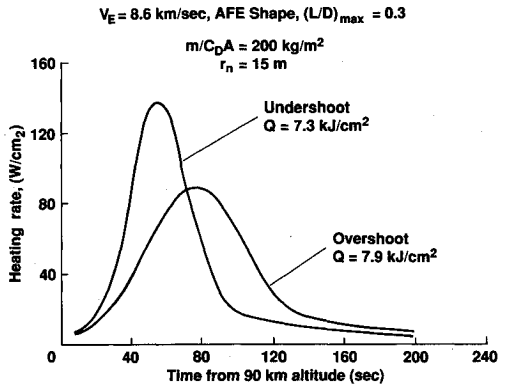

Fig. 7 Stagnation point heating pulses on AFE shape (m/C_DA = 200 kg/m²).

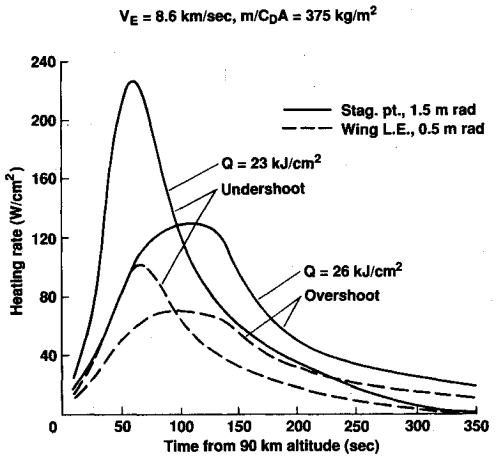

Fig. 8 Stagnation point and wing leading-edge heating pulses on delta-winged shape.

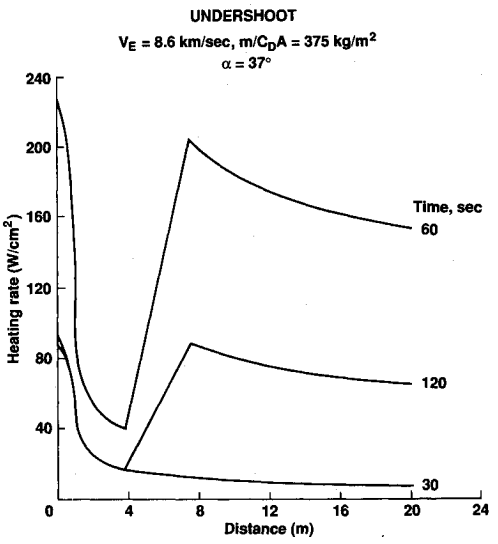

Fig. 9 Centerline heating distributions on delta-winged shape at undershoot.

path is constrained by the 5-g deceleration limit. The difference in flight path angle at the entry altitude, defined here to be 90 km, determines the corridor width. A typical set of trajectories for a maximum L/D of 0.3 and a ballistic coefficient of 100 kg/m^2 is shown in Fig. 3. The 45-km altitude of the undershoot trajectory is somewhat too low, thereby giving a peak deceleration that is slightly too high, as shown in the figure. Therefore the indicated corridor width of 1.7 deg should be about 1.6 deg.

The trajectories of the winged vehicle, which has a ballistic coefficient of 375 kg/m^2 at an angle of attack of 37 deg, are shown in Fig. 4. At a 37-deg angle of attack, the L/D is 0.85. As is to be expected, the vehicle decelerates at a lower altitude (about 38 km) and less rapidly than the previous case shown in Fig. 3. The nearly constant altitude flight path at undershoot is characteristic of vehicles having values of L/D that are greater than about 0.5. The corridor width is about 2.8 deg.

Heating

The vehicles are heated by convection and radiation. The stagnation point heating on the AFE shape is computed using an effective nose radius of 15 m. The heating pulses for the vehicle with a ballistic coefficient of 100 kg/m^2 are shown in Fig. 5. As can be seen, radiation is the dominant form of heating near peak intensity. However, the duration of the radiative pulse is much shorter than the convective one. The maximum value of the equilibrium wall temperature is about 1900 K; therefore, improved ceramic tiles can, potentially, be used for a single mission. Reduced wall catalysis has been approximately accounted for in computing the convection where the boundary layer is laminar. The finite rate wall catalysis reduces the peak stagnation point convective heating by about 25%; therefore, the peak value of the sum of convection and equilibrium radiation is decreased by 10%. Although the peak heating rate is always less at the overshoot boundary than at undershoot, the total heating load is usually higher at the former as indicated in Fig. 5 (3.5 compared with 3.2 kJ/cm^2). The heating pulse on the aft part of the forebody centerline is shown in Fig. 6. In contrast to the stagnation point, the heating shown in Fig. 6 is dominated by turbulent convection, not radiation, although the sum is about the same. A fully catalytic surface has been assumed which is consistent with turbulent boundary-layer flow measurements made in air. (Experimental measurements are needed to determine wall catalysis levels for laminar and turbulent boundary layers in CO_2.) Although the peak heating rate is about 10% higher than at the stagnation point, the total heat load at this body location is about the same as at the stagnation point.

When the ballistic coefficient is increased to 200 kg/m^2, the heating rates become too high for radiative cooling of the surface. The peak stagnation point heating rate exceeds 130 W/cm^2 (see Fig. 7) and is almost as high at the aft forebody centerline location (not shown in the figure) because the boundary layer is turbulent again. The surface is assumed to be fully catalytic since an ablator is used. (The "cold-wall" heating rates shown do not account for the influence of ablation on the boundary layer. The results presented are, therefore, independent of the heatshield material and

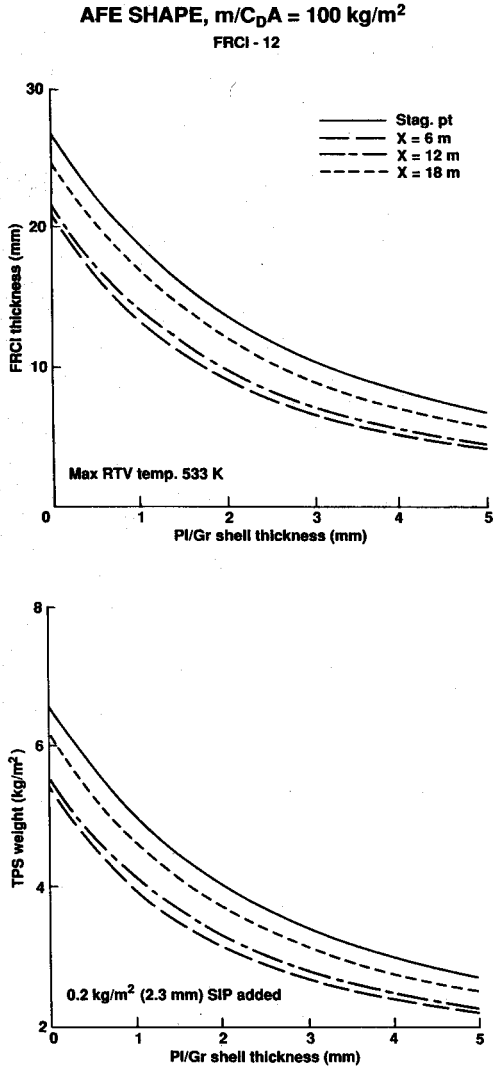

Fig. 10 TPX requirements for different skin thicknesses.

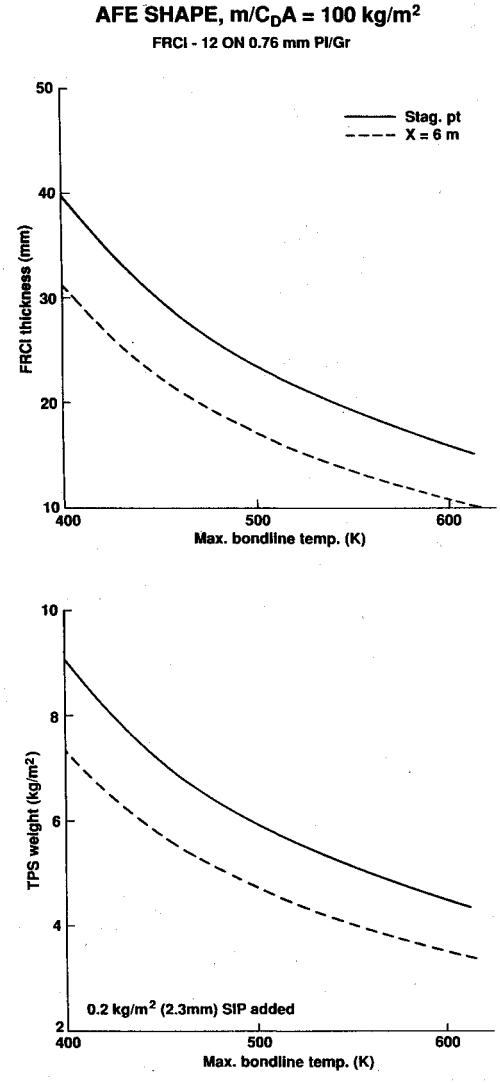

Fig. 11 TPS requirements for different skin design temperatures.

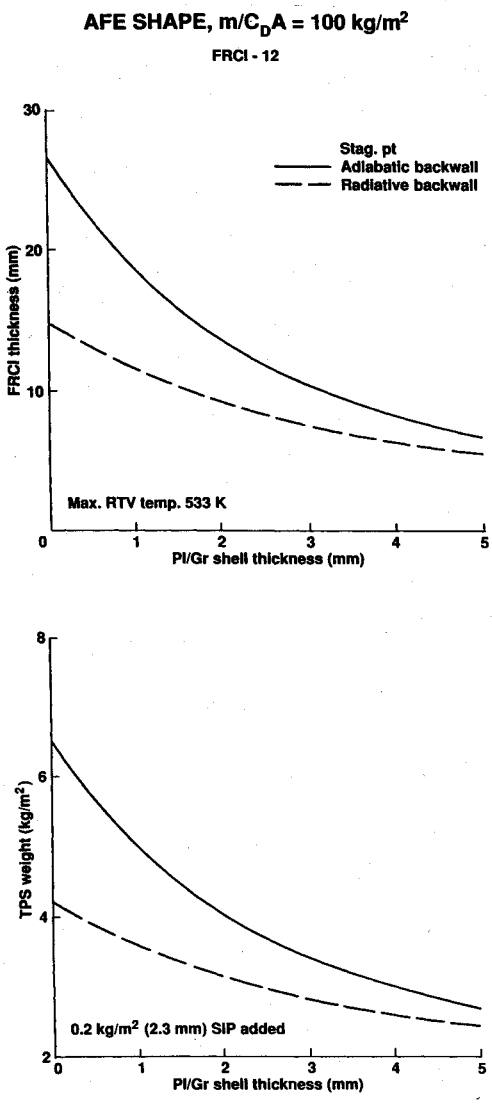

Fig. 12 TPS requirements for different backface boundary conditions.

can be used to study a variety of candidate materials.) The total heat loads are slightly more than twice the values previously shown for the lower ballistic coefficient case.

The heating rates on the winged vehicle are much higher than on the blunt shapes, primarily because the former's higher ballistic coefficient decreases the flight altitude. In addition, the winged vehicle's lower drag is achieved partially by having a much smaller nose radius (1.5 m compared with 15 m). The heating rates are shown in Fig. 8 for both the stagnation point and a point on the wing leading edge. The latter is located near midspan where the leading edge radius is 0.5 m. The peak stagnation point heating rate (combined radiative and convective) is nearly 230 W/cm^2; however, only about 20% is from radiation. The stagnation point total heat load is approximately three times higher than for the blunt, 200-kg/m^2 shape. The leading-edge heating rates are roughly one-half of the stagnation point values. The windward centerline heating rates along the undershoot boundary are illustrated in Fig. 9. Heating rate distributions are shown for 30, 60 (peak rates), and 120 s after entry. At 30 s the vehicle is at an altitude of about 57 km where the Reynolds numbers are low enough to preserve laminar flow. However, at 60 s the boundary layer is turbulent along most of the centerline, causing the peak heating rate to reach 200 W/cm^2. Although the flow remains turbulent for some time, the heating decreases as the vehicle continues to decelerate.

Heatshielding

The heatshielding or TPS requirements are analyzed by using the distributions of surface pressures and heating. For the AFE-shaped aerobrake with a ballistic coefficient of 100 kg/m^2, FRCI-12 (12 lb/ft^3 density, or specific gravity of 0.192) glass-coated tiles are considered. The peak heat flux at the outer skirt of the aerobrake is 64 W/cm^2, resulting in a peak surface temperature of about 1900 K, which is 150 K above the current temperature limit of the FRCI tiles for a single use. However, it is assumed that improvements in the temperature capability of the tiles will be realized in the future. The borosilicate glass-coated tiles are attached to the vehicle's surface with RTV adhesive. PI/Gr has a low thermal expansion coefficient, the tiles could be bonded directly to the structure if the latter is sufficiently stiff. However, the weight equivalent to a 2.3-mm (0.09-in.) thick SIP of 0.2 kg/m^2 (0.04 lb/ft^2) has been added in case the deflection of the aeroshell due to aerodynamic forces dictates the use of an SIP. Since the vehicle's skin also serves as a heat sink, tradeoffs between the tile's insulation thickness and the skin thickness have been made and are shown in Fig. 10 for several forebody locations. A bond-line design temperature of 533 K (500°F) is used and represents a conservative compromise between the temperature limits of PI/Gr and aluminum. The tradeoffs shown in Fig. 10 lead to the choice of a 0.76-mm (0.03-in.) skin thickness on each side of the honeycomb. However, an "effective" skin thickness that exceeds the actual thickness is used to approximately account for the total thermal capacitance of the honeycomb. Using an effective skin thickness of 1.3 mm (0.05 in.) requires a tile thickness of 20 mm (0.8 in.) at the stagnation point, for example. It is noteworthy that the maximum TPS thickness is required at the stagnation point, although the heating rate peaks on the forebody skirt. This occurs primarily because the pressure is highest at the stagnation point and the thermal conductivity of the tiles increases with pressure.

The effect of varying bond-line skin temperature is plotted in Fig. 11 for the previously selected skin thickness. The 533 K (500°F) temperature is near the effective limit for both RTV and the PI/Gr-aluminum honeycomb since higher temperatures degrade the structural properties. The previous calculations are based on the assumption that the backface of the aeroshell is at the adiabatic temperature. If the payload stands off significantly from the backface, large portions of the back of the aeroshell could radiate heat, thus reducing the insulation requirements. In addition, parts of the payload can act as a heat sink. The maximum potential reduction can be seen by comparing the insulation thickness shown in Fig. 12 with the values in Fig. 10. The potential weight saving has been neglected here, partly to be conservative, but also because it may be offset by afterbody heating, which has not been considered in the analysis. The results of the preceding analysis have been used to determine a forebody heatshield mass of 2960 kg or a mass fraction of 4.1%.

For the vehicles requiring ablative heatshields, a relatively brief comparison between several materials led to the choice of AVCOAT-5026. (The Apollo lunar return capsule used AVCOAT-5026. The Apollo capsule experienced heating rates and pressures that were of the same order of magnitude as the higher ballistic coefficient vehicles considered here.) AVCOAT is a low-density material (specific gravity of 0.545) consisting of an epoxy novolac resin with silica fiber reinforcement.[16] In addition to the AVCOAT ablator, a very low-density silica insulator,[13] LI-900 (specific gravity = 0.144), has been selected to protect the structure from the hot ablator. (The ceramic LI-900 constitutes the heatshield material on large portions of the Space Shuttle Orbiter.) The stagnation point on the AFE-shaped aerobrake having a ballistic coefficient of 200 kg/m^2 requires 9.5 mm (0.37 in.) of AVCOAT and 32 mm (1.25 in.) of LI-900, for example. The heatshielding off the stagnation point is based on local heating rates and one-dimensional ablation and conduction calculations. The total heatshield mass is 6580 kg, giving a mass fraction of 4.5%. The same ablative and insulative materials have also been used on the winged vehicle; however, the higher heating rates experienced by this vehicle result in a thicker heatshield. For example, the stagnation point requires 15 mm (0.6 in.) of AVCOAT and 45 mm (1.75 in.) of LI-900 insulation. On the

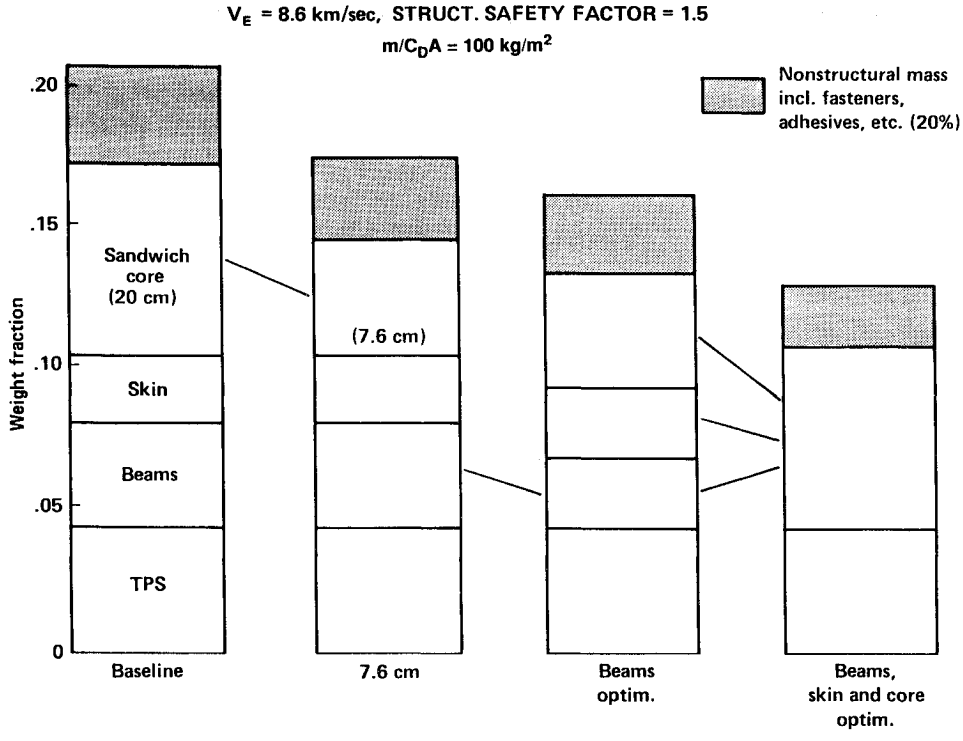

Fig. 13 Aerobrake weight fractions for AFE-shaped vehicle.

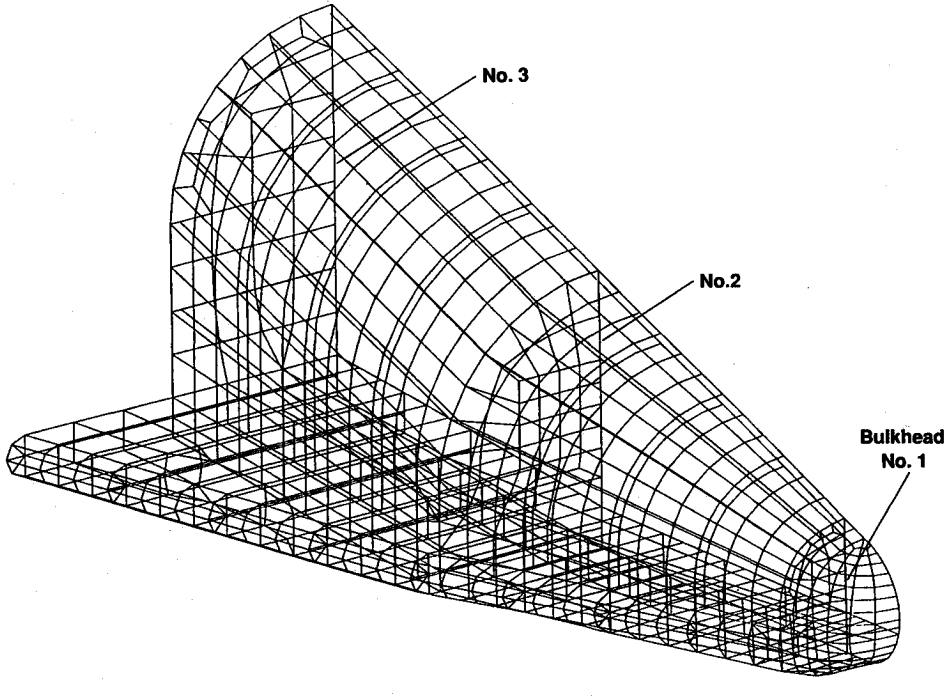

Fig. 14 Structural layout of delta-winged vehicle.

windward surface, the heatshield thicknesses are based on computations such as those shown in Fig. 9. Leeward and base heating rates are assumed to be 5% of the stagnation point values. The total heatshield mass, including the upper (leeward) parts of the vehicle and the base region, is 3310 kg or 6.1% of the vehicle's mass.

Structures

As previously stated, PI/Gr has been chosen as the structural material, although the honeycomb core is made of aluminum. (No structural properties for all PI/Gr honeycomb were found.) Two all-aluminum (2024 and 5056) honeycombs were briefly investigated but found to be heavier. The skin of the honeycomb sandwich is made of PI/Gr F174 and the core consists of AL2024. The selected skin thickness of 0.76 mm exceeds the minimum gauge thickness that is 0.5 mm. The specific gravity of the skin is 1.63 and of the honeycomb core is 0.056. The design parameters of maximum surface deflection, wrinkling, and safety factors were given in the section entitled "Analysis." The design process results are illustrated in Fig. 13 using the AFE-shaped aerobrake with a ballistic coefficient of 100 kg/m^2 as an example. The far left bar in

Fig. 13 represents the results of a baseline design study. The three structural parameters consist of the sandwich core height, the sandwich skin thickness, and the stiffener beam height. (The peak stagnation pressure is 0.10 atm.) For the baseline case, the masses of the structural components are 5061, 1769, and 2661 kg, respectively, giving a total structural mass of 9491 kg. Next the various components are optimized. First the sandwich core height is considered and reduced from 20 cm (8 in.) to 7.6 cm (3 in.), resulting in a saving of 2026 kg. The beams are considered next, and their mass is reduced by 864 kg. Finally, the combined structure is optimized to achieve a further reduction of 1956 kg. The total reduction of mass from the baseline design is 51% for a final structural mass of 4645 kg. The heatshield, or TPS, mass is added and, in addition, a 20% contingency to account for nonstructural mass such as various types of fasteners, fittings, and filling, etc. (Note that the nonstructural mass contingency is also applied to the TPS to be conservative.) However, to account for a significant uncertainty in the fraction that must be devoted to nonstructural mass, values of both 20 and 40% are used. The final aerobrake mass is 9130 kg, or 12.6% of the gross weight of the vehicle for the 20% nonstructural mass contingency, and 10,650 kg, or 14.6% when 40% contingency is used.

The previous procedure was repeated for the heavier AFE-shaped vehicle (which experienced a peak stagnation pressure of 0.183 atm) and yielded a structural mass of 7400 kg. After adding the TPS mass and adding the nonstructural mass contingencies of 20 and 40%, the aerobrake masses are 16,780 and 19,570 kg, respectively. The corresponding mass fractions for the aerobrake are 11.5 and 13.5%.

The winged vehicle's structure is also assumed to be made primarily of PI/Gr. The structure consists of a honeycomb shell, reinforced by three bulkheads, reinforcement frames, and longitudinal beams and stiffeners. The structural layout, including the location of the three bulkheads in the fuselage, is shown in Fig. 14. The configuration is optimized for minimum weight by varying the sandwich skin thickness, the core depth, and the ring frame and beam cross-sectional dimensions without overstressing any part of the structure. (A peak stagnation pressure of 0.272 atm is used.) For a honeycomb skin thickness of 1 mm, a (minimum gauge) core height of 12.7 mm is found to be optimum. The final structural weights are 2015 kg of skin and beam material and 1150 kg of honeycomb core, for a total mass of 3165 kg. The entire external portion of the vehicle, consisting of wings and fuselage, but excluding the payload that is housed inside the fuselage, is considered to be the "aerobrake" from the standpoint of mass calculation. Adding the TPS mass of 3310 kg and nonstructural mass contingencies of 20 and 40% yields total masses of 7770 and 9065 kg, respectively. The corresponding structural, plus TPS, mass fractions are 14.2 and 16.6%. The winged configuration has a somewhat higher vehicle mass fraction than those found for the blunt shapes because of the former's much higher ballistic coefficient. The higher ballistic coefficient of the winged vehicle leads to enhanced heating, especially turbulent convection on the windward surface, and thus a higher TPS mass fraction.

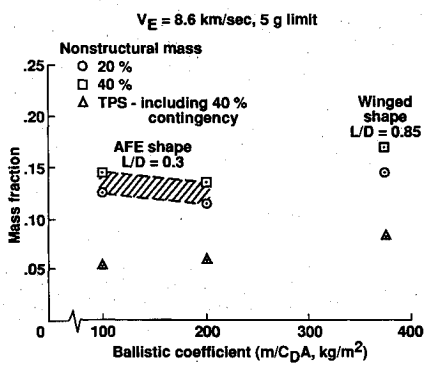

Fig. 15 Mass-fraction summary for two manned Mars mission aerobraking shapes.

The final results for both vehicle shapes are summarized in Fig. 15, where the effect of assuming both 20 and 40% nonstructural mass contributions can be seen also. When the conservative nonstructural mass contributions of 40% are applied to both the structure and the TPS, the aerobrake mass fractions range from 13.5 to 14.6% for the AFE shapes, and for the winged vehicle the mass fraction is 16.6%.

It is instructive to compare the previous weight fractions with those calculated by Boeing.[20] Boeing used an entry velocity of 7.4 km/s and a peak deceleration limit of 6 Earth g. Although the configuration of the aerobrake resembles the AFE shape, it is flown at a higher angle of attack than AFE to yield a peak L/D of 0.5. The total mass is about 100 mt, resulting in a ballistic coefficient of 394 kg/m^2. The Boeing design is based on the use of graphite/magnesium metal-matrix spars and titanium/aluminum sandwich panels. The structure has not been optimized for minimum weight at this time. The total aerobrake mass fraction is 18.9%, of which 3.3% is TPS. The structural mass fraction is larger than the values presented here for the blunt aerobrakes partly because Boeing used a 1-g higher deceleration limit and did not yet optimize the structure, or materials, to minimize weight. Boeing's lower TPS mass fraction can be attributed to their 1.2 km/s lower entry velocity. The mass fractions are in reasonable agreement when the differences in the design conditions between the blunt aerobrakes studied here and Boeing's design are considered.

To put the aerobrake mass fractions into perspective, the mass fraction that would be required if propulsive braking were used has been estimated. Assuming that the most efficient current chemical propellants consisting of liquid hydrogen and oxygen are used, a mass fraction of about 65% has been calculated for the propulsive system and fuels.

Concluding Remarks

The vehicle's mass fractions that must be devoted to the aerobrakes, including the heatshields, have been computed for Mars entry at 8.6 km/s. Blunt low L/D, AFE-shaped configurations with ballistic coefficients of 100 and 200 kg/m^2 have been studied. After adding heatshielding and optimizing the aerobrakes' structure, its total mass fraction was found to vary from about 15 to 13% for ballistic coefficients of 100 and 200 kg/m^2, respectively. A winged vehicle with a medium L/D has also been studied and was found to have a structural plus heatshield mass fraction of slightly less than 17%. The aerobrakes' mass fractions are less than one-quarter of the mass fractions that would be required for propulsive braking at a speed of 8.6 km/s using the most advanced current chemical propellants.

Acknowledgments

The authors thank the following of their colleagues: J. O. Arnold, Chief of the Thermosciences Division, and D. M. Cooper, Chief of the Computational Chemistry Branch, for initiating and supporting the study, respectively; J. E. Lyne, for calculating several of the overshoot and undershoot trajectories; and Howard Goldstein and Gene Menees for valuable editorial comments.

References

[1]Syvertson, C. A., and Dennis, D. H., "Trends in High-Speed Atmospheric Flight," AIAA Paper 64-514, July 1964.

[2]Tauber, M. E., and Seiff, A., "Optimization of Heating of Conical Bodies Making Lifting Hyperbolic Entries into the Atmospheres of Earth and Mars," AIAA CP-9, Oct. 1964.

[3]Clark, B., "Manned Mars Missions for the Year 2000," AIAA Paper 89-0512, Jan. 1989.

[4]Braun, R. D., and Blersch, D. J., "Propulsive Options for a Manned Mars Transportation System," AIAA Paper 89-2950, Jan. 1989.

[5]Menees, G. P., "Aeroassisted-Vehicle Design Studies for Manned Mars Missions," International Astronautical Federation/International Academy of Astronautics, IAF/IAA Paper 87-433, Oct. 1987.

[6]Lyne, J. E., "Physiologically Constrained Aerocapture for Manned Mars Missions," NASA TM 103954, Aug. 1992.

[7]Tauber, M. E., Bowles, J. V., and Yang, L., "The Use of Atmospheric Braking During Mars Missions," *Journal of Spacecraft and Rockets*, Vol. 27, No. 5, 1990, pp. 514–521.

[8]Softley, E. J., Graber, B. C., and Zempel, R. E., "Experimental Observation of Transition of the Hypersonic Boundary Layer," *AIAA Journal,* Vol. 7, No. 2, 1969, pp. 257–263.

[9]Tauber, M. E., and Adelman, H. G., "Thermal Environment of Transatmospheric Vehicles," *Journal of Aircraft,* Vol. 25, No. 4, 1988, pp. 355–363.

[10]Lee, J. S., and Bobbitt, P. J., "Transport Properties at High Temperatures of CO_2-N_2-O_2-Ar Gas Mixtures for Planetary Entry Applications," NASA TN D-5476, Nov. 1969.

[11]Tauber, M. E., and Sutton, K., "Stagnation Point Radiative Heating Relations for Earth and Mars Entries," *Journal of Spacecraft and Rockets,* Vol. 28, No. 1, 1991, pp. 40-42.

[12]Nicolet, W. E., "User's Manual for the Generalized Radiation Transfer Code (RAD/EQUIL)," NASA CR-116353, Oct. 1969.

[13]Chiu, S. A., and Pitts, W. C., "Reusable Surface Insulations for Reentry Spacecraft," AIAA Paper 91-0695, Jan. 1991.

[14]Cullimore, B., Goble, R., Jensen, C., and Ring, S., "SINDA 85/FLUINT-Systems Improved Numerical Differencing Analyzer and Fluid Integrator User's Manual," Martin Marietta Corp., Denver, CO, Aug. 1986.

[15]Kendall, R. M., Bartlett, E. P., Rindal, R. A., and Moyer, C. B., "An Analysis of the Coupled Chemically Reacting Boundary Layer and Charring Ablator (Parts I–VI)," NASA CR-1060–1065, June 1968.

[16]Henline, W. D., "Aerothermodynamic Heating Environment and Thermal Protection Materials Comparison for Manned Mars-Earth Return Vehicles," AIAA Paper 91-0697, Jan. 1991.

[17]Anon., "MSC/NASTRAN User's Manual for Version 66," McNeil-Schwendler Corp., Los Angeles, CA, 1989.

[18]Pindera, M. J., and Herakovich, C. T., "An Endochronic Theory for Transversely Isotropic Fibrous Composites," Virginia Polytechnic Inst. and State Univ., VPI-E-81-27, Blacksburg, VA, 1981.

[19]Papadopoulos, P., Tauber, M. E., and Chang, I. D., "Heat Shield Erosion in a Dusty Martian Atmosphere," *Journal of Spacecraft and Rockets,* Vol. 30, No. 2, 1993, pp. 140–151.

[20]Anon., "Space Transfer Concept and Analysis for Exploration Missions," Boeing Defense and Space Group, Advanced Civil Space Systems, Rept. D615-10030-2, Huntsville, AL, March 1991.